Electronic structure and charge transfer processes in a Bi-Ca misfit cobaltate

E. Carleschi,[1,2,*] M. Malvestuto,[3] M. Zacchigna,[2] A. Nicolaou,[4] V. Brouet,[4] S. Hébert,[5] H. Muguerra,[5] D. Grebille,[5] and F. Parmigiani[1,2,†]

[1]*Dipartimento di Fisica, Università degli Studi di Trieste, via A. Valerio 2, 34127 Trieste, Italy*

[2]*TASC INFM–CNR National Laboratory, S.S. 14 km 163.5, Area Science Park, Basovizza, 34012 Trieste, Italy*

[3]*Sincrotrone Trieste, S.S. 14 km 163.5, Area Science Park, Basovizza, 34012 Trieste, Italy*

[4]*Laboratoire Physique des Solides, UMR 8502, CNRS, Université Paris-Sud, Bâtiment 510, 91405 Orsay, France*

[5]*Laboratoire CRISMAT, UMR 6508 CNRS-ENSICAEN, 6, Boulevard du Maréchal Juin, 14050 Caen Cedex, France*

(Received 13 January 2009; published 13 July 2009)

We report polarization-dependent on-resonance and off-resonance photoemission and x-ray absorption measurements to probe the character and the symmetry of the occupied and empty valence-band (VB) states of the four-layered misfit cobaltate $[Bi_2Ca_2O_4]^{RS}\cdot[CoO_2]_{1.67}$. These experiments bring clear evidence that the one-electron removal VB photoemission spectra, between the Fermi energy (E_F) and ~4.5 eV, contain Co $3d$ states, which are strongly hybridized with O $2p$ states in the binding energy region of ~1.8– ~4.5 eV below E_F. The states at the Fermi energy have a_{1g} out-of-plane symmetry. In addition, by tuning the incident photon energy across the Co $2p_{3/2}\rightarrow$Co $3d$ (a_{1g}) threshold and the O $1s\rightarrow$O $2p$–Co $3d$ (a_{1g}) hybridized threshold, both found at ~2 eV below the absorption edge maximum, it is possible to observe a transition from a Raman regime to an Auger regime. From this transition the charge transfer dynamics from the Co $3d$ to the O $2p$ states and from the O $2p$ to the Co $3d$ states have been estimated to be ~3 and ~3.3 fs, respectively. This combined information suggests an electron hopping process between neighboring Co a_{1g} states across E_F and mediated by O $2p$ states with suitable symmetry.

DOI: 10.1103/PhysRevB.80.035114 PACS number(s): 71.20.Be, 71.27.+a, 79.60.−i

I. INTRODUCTION

In the last decade sodium and misfit cobaltates have challenged our understanding of the physics of strongly correlated materials because of the coexistence of large thermoelectric power (TEP) with low resistivity and low thermal conductivity.[1–7] Misfit cobaltates are characterized by a complex three-dimensional crystalline structure with a rocksalt (RS) block of oxides in between CoO_2 slabs. In the Bi misfit family, the RS block is formed by four pseudoquadratic layers of the type M-O/Bi-O/Bi-O/M-O (with M=Ba, Sr, or Ca) [see Fig. 1(a)]. By reducing the electron motion along the c axis, the RS imposes a quasi-two-dimensionality upon the CoO_2 planes and acts as a charge reservoir for the CoO_2 layers. The composition of the RS block modifies the number of free carriers in the CoO_2 planes and consequently the nominal ratio of Co^{3+} to Co^{4+} ions. Angle-resolved photoemission spectroscopy (ARPES) measurements have shown that the electronic structure near the Fermi level is similar in Na and misfit cobaltates, which legitimates the comparison.[8]

Here we report an experimental study, based on polarization-dependent (on-resonance and off-resonance) photoemission (PE) and x-ray absorption spectroscopy (XAS), of the Bi misfit cobaltate $[Bi_2Ca_2O_4]^{RS}\cdot[CoO_2]_{1.67}$ (hereafter BiCaCoO). The aims of this work are to elucidate the nature and the character of the Co $3d$ occupied and unoccupied valence-band (VB) electronic states and to evaluate the degree of hybridization of the Co-O bonds. In addition, by combining resonant photoemission (ResPES) and XAS with the polarization selection rules, we also obtain information about the symmetry of the resonating states. ResPES measurements at the Co L_3 and Co M_{32} edges reveal strong Co $3d$ character down to ~4.5 eV binding energy (BE) and a significant overlap between states with Co $3d$ and O $2p$ characters between 1.8 and 4.5 eV below E_F. These measurements, together with polarization-dependent PE and XAS measurements, confirm that the occupied and empty states across E_F have a_{1g} out-of-plane symmetry. We also track the Raman-Auger transition for Co $2p_{3/2}3d3d$ and O $1s2p2p$ Auger peaks. Both these transitions involve the Co a_{1g} out-of-plane states, revealing an abrupt delocalization of the ex-

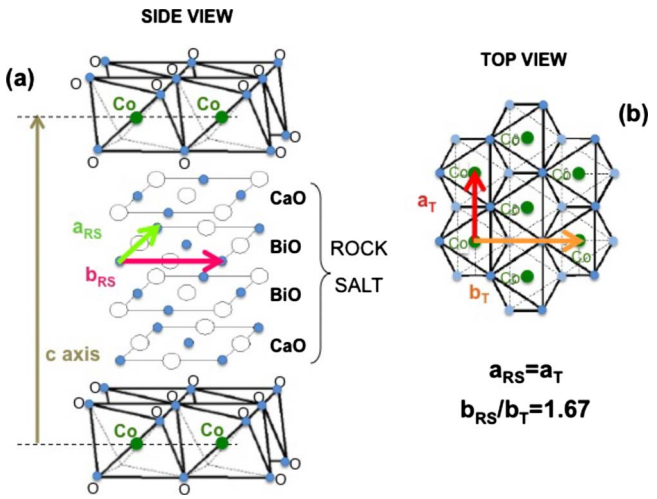

FIG. 1. (Color online) (a) Schematic of the side view of the BiCaCoO misfit structure. The distorted Co-O octahedra layers are separated by four pseudoquadratic RS layers stacked in the order CaO/BiO/BiO/CaO. a_{RS} and b_{RS} indicate the in-plane crystallographic axes for the RS. (b) Top view picture of the CoO_2 triangular lattice. The green circles are the Co ions, while light blue circles are the O ions. a_T and b_T indicate the in-plane crystallographic axes for the triangular lattice.

cited core electrons. Within the sudden approximation, this finding can be interpreted in view of the electron transport mechanism, suggesting an electron hopping process between neighboring Co a_{1g} states across E_F and mediated by O $2p$ states with a suitable symmetry. The charge transfer times are estimated to be ~3 fs for electrons from Co $3d$ to O $2p$ states and ~3.3 fs for electron transfer from O $2p$ to Co $3d$ states.

The physical properties of BiCaCoO are shown in Ref. 4. Its room-temperature (RT) TEP (~140 μV K^{-1}) is comparable with that of Na_xCoO_2 with x near 0.8 (Ref. 5) and larger than BiSrCoO (Ref. 9) (~125 μV K^{-1}) and BiBaCoO (~95 μV K^{-1}).[10] Due to the low value of its thermal conductivity (~1 W K^{-1} m^{-1} at 300 K), its figure of merit is calculated to be 0.015 at RT, comparable with that of Na_xCoO_2 (0.03) and that BiSrCoO (0.025). The doping in BiCaCoO, estimated to $x \approx 0.8$ (Ref. 11) to 0.9,[8] has the largest x value for misfit cobaltates. This puts BiCaCoO in the poorly explored region of the Na_xCoO_2 phase diagram, near the band insulator limit, where unexpected magnetic correlations and a huge increase in the TEP (Ref. 5) are detected. The in-plane resistivity $\rho_{ab}(T)$ (60 mΩ cm^{-1} at RT) exhibits a progressive change from $d\rho_{ab}/dT > 0$ to $d\rho_{ab}/dT < 0$ at $T \sim 200$ K as T decreases. BiCaCoO shows a large negative magnetoresistance[4,10,12] (not reported in Na cobaltates) reaching −87% in 7 T at 2.5 K—the largest value reported for a misfit cobaltate—revealing that there exists a coupling between itinerant carriers and magnetic fluctuations. These properties are consistent with those of samples grown by other groups.[13,14] To interpret these physical properties, the modification of the orbital occupation near the top of VB has been proposed[12] and a clear picture of the nature of the electronic states at the top of the VB is desirable.

Figure 1(a) shows a representative picture of the BiCaCoO misfit structure. The RS block separates Co-O layers, in which Co ions are located in the center of an octahedron with six oxygen atoms. Each octahedron is tilted and compressed with respect to the c axis. Such a distortion results in layers of triangular arrays of Co sandwiched between oxygen layers [see Fig. 1(b)], which are also present in Na and other misfit cobaltates. The misfit structure derives from the incommensurability of one of the in-plane cell parameters between each sublattice ($b_{RS}/b_T = 1.67$).[15] The octahedral distortion lowers the local symmetry group of cobalt from O_h (octahedral) to D_{3d} (trigonal), leading the occupied t_{2g} states to split into new states, one with out-of-plane symmetry (a_{1g}) and the other double degenerate with more in-plane symmetry (e_g') compared with a_{1g}. These states can be represented as

$$|a_{1g}\rangle = \frac{1}{\sqrt{3}}[|d_{xy}\rangle + |d_{yz}\rangle + |d_{zx}\rangle], \quad (1)$$

$$|e'_{g1}\rangle = + \frac{1}{\sqrt{3}}[|d_{xy}\rangle + e^{-i2\pi/3}|d_{yz}\rangle + e^{-i4\pi/3}|d_{zx}\rangle], \quad (2)$$

$$|e'_{g2}\rangle = - \frac{1}{\sqrt{3}}[|d_{xy}\rangle + e^{+i2\pi/3}|d_{yz}\rangle + e^{+i4\pi/3}|d_{zx}\rangle], \quad (3)$$

where $|d_{xy}\rangle$, $|d_{yz}\rangle$, and $|d_{zx}\rangle$ are the atomic orbitals in the reference system (x,y,z) of the undistorted octahedra. Clear pictures of these orbitals are reported in Fig. 2 in Ref. 16.

The knowledge of the energetic order between the t_{2g} orbitals is of crucial importance for understanding the interplay between the low-energy electrodynamics properties of these compounds and the symmetry character of the carriers.[3–5,13,17,18] Although, in a crystal-field approach the trigonal distortion would stabilize the a_{1g} state compared to e_g' states,[19] band calculations[20] predict that the top of the t_{2g} band has a dominant a_{1g} character, with six e_g' pockets at K points of the Brillouin zone. Many spectroscopic experimental studies[21–23] confirm the a_{1g} character prediction, but e_g' pockets could not be detected by ARPES.[8,24–28] *Ab initio* quantum chemistry calculations predict a lower value for e_g' bands,[29] which may account for this difference. Nevertheless, a direct and clear experimental evidence of the out-of-plane symmetry character of the states across E_F is lacking in misfit cobaltates.

II. EXPERIMENTAL

BiCaCoO single crystals with dimensions of approximately $1.5 \times 1.5 \times 0.3$ mm^3 ($a \times b \times c$) were grown by a standard flux method.[30] They were characterized by magnetic and transport measurements,[10] while the misfit crystal structure and parameters have been investigated by x-ray diffraction measurements confirming the misfit crystal structure.[15]

The PE and XAS experiments were carried out at the BACH beamline[31,32] on the Elettra storage ring. Samples were cleaved *in situ* at RT at a background pressure of $< 5 \times 10^{-10}$ mbar, while the experiments were performed in a background pressure of $< 4 \times 10^{-10}$ mbar. The cleaved surfaces were seen to be very stable and remained clean for ~48 h.

PE spectra were acquired using a 150 mm VSW hemispherical electron analyzer with a 16-channel detector. The analyzer work function ϕ was determined by measuring the E_F of a pure Au sample using the first and the second orders of the diffraction grating. The overall experimental resolutions were set at 380, 250, and 70 meV for ResPES spectra across the Co L_3 edge, the O K edge, and the Co M_{32} edges, respectively. XAS spectra were measured using the total electron yield with energy resolutions of 0.5 and 0.2 eV for the Co L_{32} edges and the O K edge, respectively. PE and XAS spectra were referred to the E_F of a gold reference sample. All data were collected at RT.

Figures 2(a) and 2(b) show the polarization configurations exploited. The incidence angle (θ_{inc}), defined as the angle between the direction of the incoming photon direction and the normal to the sample surface (i.e., the c axis), was fixed at 60° for all PE measurements, while it was changed from 0° to 60° for XAS measurements. Hereafter we define as the P geometry the experimental condition when the light electric field $\vec{E}$ lies in the plane defined by the photon direction and the c axis [Fig. 2(a)] and the S geometry when $\vec{E}$ is perpendicular to that plane [Fig. 2(b)]. Figure 2(c) shows the scheme of the light electric field components with respect to the orientation of the Co-O octahedra. Note that in the P geometry there are contributions from out-of-plane states of

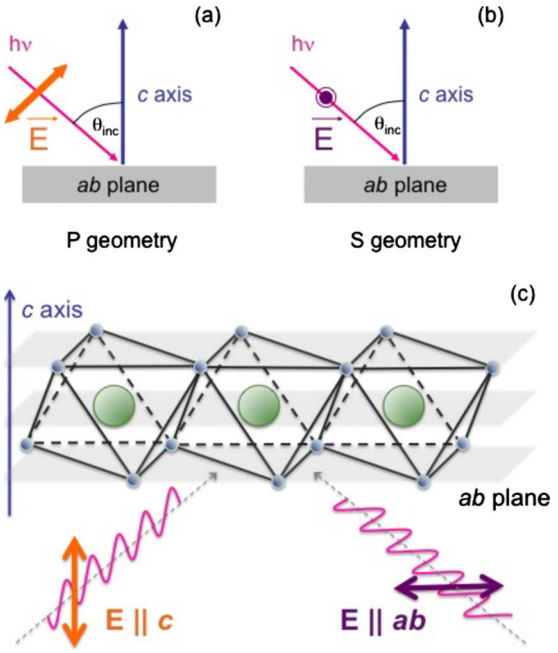

FIG. 2. (Color online) Schematic view of the experimental configurations: (a) in the P geometry the light polarization is parallel to the plane defined by the photon direction and the c axis; (b) in the S geometry the light polarization is perpendicular to it. (c) Scheme of the light electric field components with respect to the orientation of the Co-O octahedra.

a_{1g} symmetry together with the in-plane e_g' states.

PE spectra taken on the same sample, for different cleaves, were found to be consistent. The cleanliness of the surface was checked during the entire experiment by taking PE spectra of the VB and O 1s spectral region. The O K and Co L_{32} ResPES spectra were aligned using the Bi $5d_{5/2}$ core level.

III. X-RAY ABSORPTION RESULTS

Figure 3(a) shows the first peak of the O K edge absorption spectra acquired in the P geometry at $\theta_{inc}=0°$ and $\theta_{inc}=60°$. According to the literature on Na cobaltates,[33,34] the features labeled as A_1, A_2, and A_3 and located at 528.1, 529, and 530 eV, respectively, are assigned to O 2p empty states hybridized with Co 3d empty state, while the structures at higher photon energies [shown in the inset of Fig. 3(a)] are assigned to transitions from the O 1s to O 2p empty states hybridized with Bi and Ca outer orbitals (532–539 eV) and with Co 4sp continuum states (539–547 eV). The energy splitting between A_1 and A_2 is ~0.9 eV and that between A_2 and A_3 is ~1 eV. The angular dependence of their intensities (an increase in spectral weight with the incidence angle for A_1 and an opposite trend for A_2) allows to specifically assign them to Co^{4+} a_{1g} (A_1), Co^{3+} e_g (A_2), and Co^{4+} e_g (A_3) states, as was done for Na cobaltates.[33] It is worth noting that the angular dependence of A_3 is not straightforward because of the eventual presence of O 2p–Bi 6p hybridized states in the same energy region, as already reported in Refs. 21 and 23 for BiSrCoO and confirmed by cluster calculations for BiCaCoO.[35]

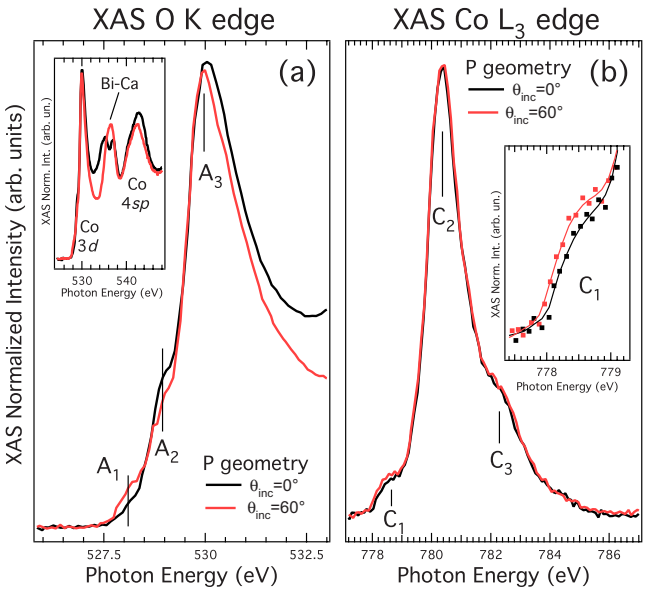

FIG. 3. (Color online) (a) O K edge main peak and(b) Co L_3 edge XAS spectra of BiCaCoO acquired in the P geometry for $\theta_{inc}=0°$ (black curve) and $\theta_{inc}=60°$ (red curve). The inset in (a) shows the wide O K edge absorption spectrum. The inset in (b) shows enlarged C_1 feature; dots represent the experimental points, while the dashed lines represent the smoothed curves. A linear background has been subtracted to the spectra, and they have been consequently normalized at 1 at 555 eV for the O K edge and 815 eV for the Co L_3 edge, far above the absorption threshold.

Co L_3 edge XAS spectra at $\theta_{inc}=0°$ and $\theta_{inc}=60°$ are shown in Fig. 3(b). They are also in good experimental agreement with those reported for other cobaltates.[21,33,34,36] L_3 edge consists of a main peak at 780.3 eV (C_2) and two shoulders at 778.5 eV (C_1) and 782.5 eV (C_3), which can be attributed to Co^{4+} ions, by analogy with Na cobaltates.[33,34] This confirms qualitatively the doping estimated for BiCaCoO. The data show an increasing emission for the C_1 feature by increasing the incident angle [see inset of Fig. 3(b)]. This result confirms that the holes near E_F have a dominant a_{1g} out-of-plane orbital character, in agreement with O K edge XAS.

IV. PHOTOEMISSION RESULTS

A. Valence-band features

Figure 4 reports the full VB spectrum of BiCaCoO acquired at $h\nu=90$ eV in the P geometry. The most-pronounced VB components are marked by the letters from A to G. The broad emission centered at 11 eV is the result of the superposition of two components: the Bi 6s core level[37] (H) at ~11.5 eV and the correlation satellite G centered at ~10.5 eV BE (detected also in Na cobaltates)[24] and not predicted by density of states (DOS) calculations,[20] indicating a strongly correlated behavior.

By comparing this spectrum with that of $Na_{0.7}CoO_2$ (Ref. 24) measured at the same photon energy, one can see that the VB line shape reveals the same general features as Na cobaltates: a peak near the Fermi level is separated from a

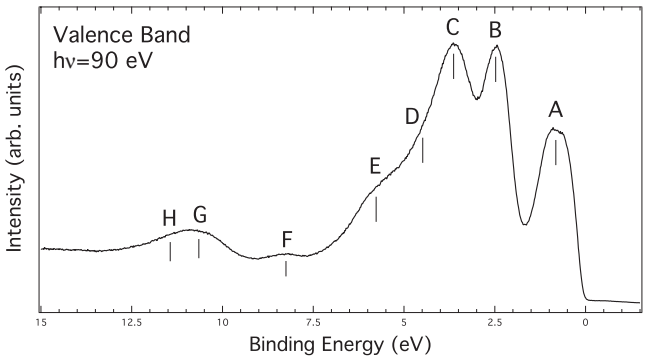

FIG. 4. BiCaCoO VB spectrum acquired at RT with $h\nu$ =90 eV in the P geometry (overall resolution: 70 meV).

wider structured region from ~2 to ~8 eV BE even if it has more structure with respect to Na. This is in general agreement (with the exception of emission F) with band theory DOS calculations[20] for $Na_{0.5}CoO_2$, confirming that VB states are constituted mainly by Co 3*d* and O 2*p* states. In the following we will explain the character and the symmetry of the VB states.

B. ResPES at the Co L_3 edge

Panels (a) and (b) of Fig. 5 show a selection of wider VB spectra obtained by tuning the photon energy across the Co L_3 edge from 775 to 785.5 eV in the P and S geometries. The photon energies are marked as circles on the corresponding XAS spectra in panels (c) and (d). The spectra have been normalized to the intensity of the Bi $5d_{3/2}$ core level, located at 28.7 eV BE, whose cross section does not change appreciably in this energy range. By increasing the photon energy for both P and S geometries the emission near E_F is first almost suppressed ($h\nu \simeq 777$ eV) and then it strongly increases, starting from $h\nu \simeq 779$ eV, reaching a maximum at the top of the absorption edge, $h\nu \simeq 780.2$ eV. This finding is consistent with that reported for Co L_3 ResPES experiments on the superconductor $Na_{0.35}CoO_2 \cdot 1.3H_2O$ (Ref. 22) and the Bi-Sr misfit cobaltate.[23] This result confirms that the sharp emission near E_F has a predominant Co 3*d* t_{2g} character.

The constant BE pure resonant enhancement of the deeper part of the VB (2–9 eV BE) cannot be clearly interpreted because of the resonant Co $2p_{3/2}3d3d$ Auger line [marked by thick vertical dashes in Figs. 5(a) and 5(b)]. The evolution of the Auger contribution will be discussed in Sec. V A.

Figure 6(a) shows the resonant spectral weight (RSW) obtained by subtracting spectrum 1 from spectrum 8 in Figs. 5(a) and 5(b). The amount of resonance of the peak near E_F is less pronounced in the S geometry than in the P geometry. This effect is unlikely to originate from geometric factors, i.e., the enhancement of the PE cross section for out-of-plane a_{1g} states in the P geometry with respect to e_g'. In fact, the graph also reveals a transfer of spectral weight from the peak near E_F to the resonant Co $2p_{3/2}3d3d$ Auger line in the S geometry with respect to the P geometry. The more intense Auger emission in the S geometry with respect to the P geometry can be regarded as experimental evidence that the

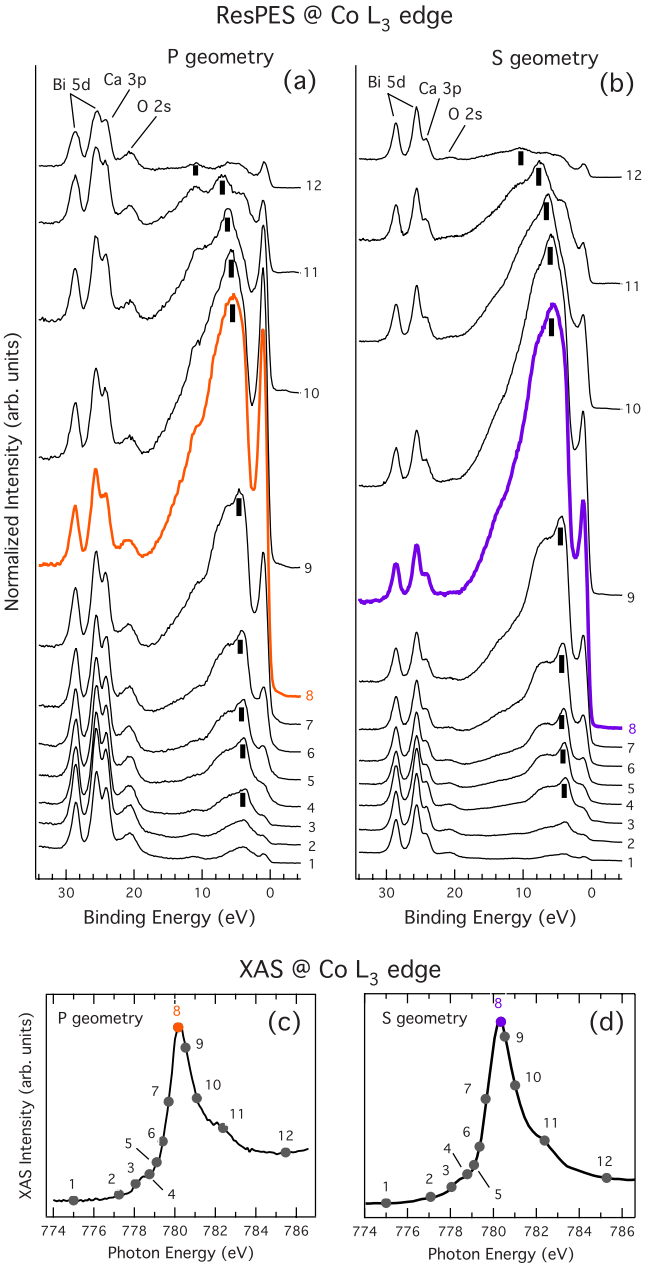

FIG. 5. (Color online) Resonant VB PE spectra collected with photon energies across the Co L_3 edge in the (a) P and (b) S geometries. The spectra corresponding to the resonance maximum are shown in thick lines (orange and violet, respectively). XAS spectrum at the Co L_3 edge measured in the (c) P and (d) S geometries.

in-plane empty states are more delocalized than those out of plane.

C. Geometry dependence of the valence band

In order to evaluate the energetic order of the Co 3*d* t_{2g} states near E_F, we performed high-resolution off-resonance VB measurements at $h\nu$=94 eV. The results are shown in Fig. 6(b) for both the geometries. The comparison between the two spectra shows that in the S geometry the spectral weight near E_F decreases, while it increases in the P geom-

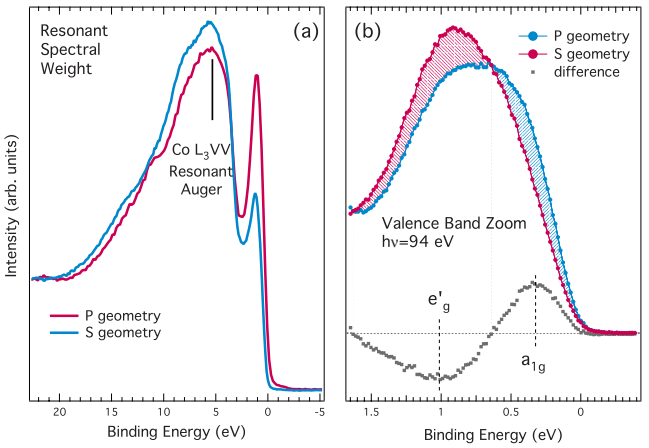

FIG. 6. (Color online) (a) Resonant spectral weight for the P and S geometries obtained by subtracting spectrum 1 from spectrum 8 in Figs. 5(a) and 5(b). The spectra have been normalized to the background taken at 30 eV BE. (b) Polarization-dependent VB PE spectra acquired at $h\nu$=94 eV with an overall resolution of 70 meV; the difference spectrum (P geometry–S geometry) permits to identify the a_{1g} and e'_g centroids.

etry. This behavior is consistent for VB acquired at different photon energies (not shown here). This shows unambiguously that the low-lying excitations have majority out-of-plane a_{1g} character in BiCaCoO as in other cobaltates. By taking the difference between these two spectra, we can estimate that the centroids of the a_{1g} and e'_g bands lie at ~0.33 and ~1 eV below E_F, so the energy difference between the centroids of the two bands is not large (~670 meV), and the bands largely overlap over the 1 eV peak below E_F. This energy splitting is not large enough to reduce from six to two the spin degeneracy of the hole in the VB.

D. ResPES at the Co M_{32} edges

Figure 7 shows the modulation of the VB, while the photon energy is tuned across the Co M_{32} edges in both (a) P and (b) S geometries (the Co 3p core level main peak is located at about 60 eV BE). A Shirley background[38] has been subtracted from the normalized spectra. As the ResPES at Co L_3 edge is difficult to interpret due to the superposition of the Auger signal, resonant effect at this edge can be used to get complementary information. The VB components are marked by the letters from A to G according to the assignment in Fig. 4. Transition metal 3p-3d resonances are usually much less intense than the 2p-3d resonances and sometimes difficult to interpret. However, here ResPES spectra reveal clear resonant behavior. In fact, emission B, whose centroid is located at 2.37 eV BE, resonates in the P geometry reaching a maximum at $h\nu$=68 eV, while emission C, located at 3.4 eV BE, resonates in the S geometry reaching a maximum at $h\nu$=65 eV [these two spectra are plotted together in Fig. 7(c)]. So the Co 3d character extends up to ~4.5 eV below. This indicates not only that components B and C contain Co 3d character but also that they have different symmetries, B being more out of plane and C being more in plane. Their resonant behaviors at different energies are due to the different symmetries of their wave functions.

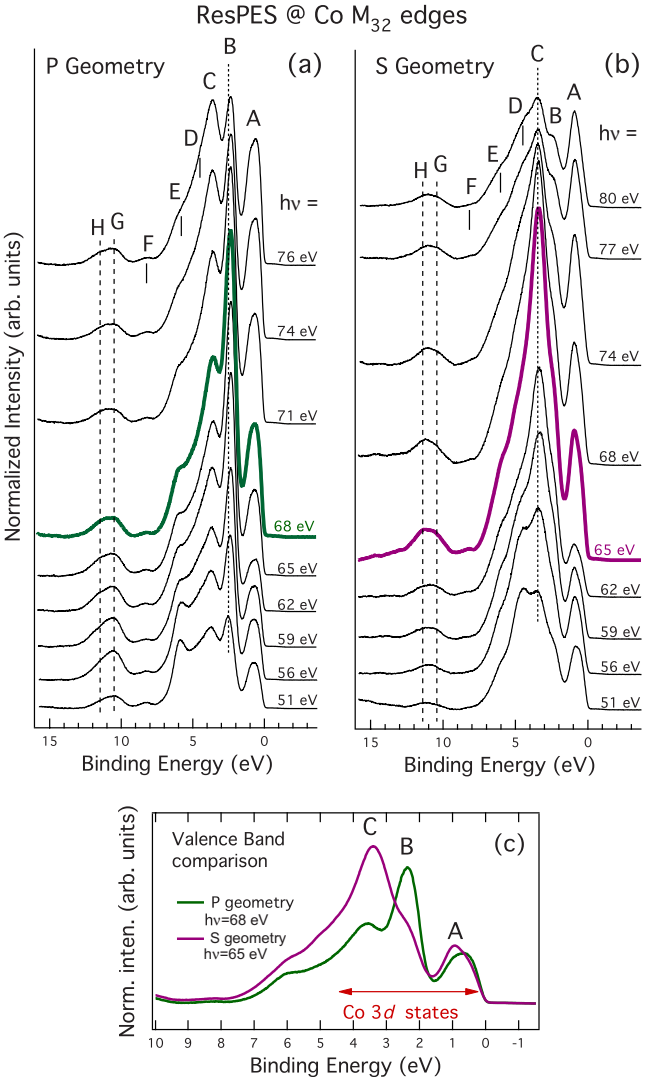

FIG. 7. (Color online) ResPES spectra collected with photon energies across the Co M_{32} edges in the (a) P and (b) S geometries. The spectra corresponding to the resonance maximum are shown in thick lines. (c) Comparison between the resonance maximum in the P geometry ($h\nu$=68 eV) and in the S geometry ($h\nu$=65 eV).

The resonant enhancement of these two emissions is identified by their corresponding resonant profiles (RPs) across the Co M_{32} edges, shown in Figs. 8(a) and 8(b) for all the VB components. RP have been calculated by integrating the intensity of each VB component as a function of the incident photon energy and normalizing such intensity to the overall VB intensity. This makes the profiles to represent the relative enhancement of each emission with respect to the overall VB spectral weight that, due to the partial photoionization cross section of the VB, becomes weaker as the excitation energy increases.

Of particular interest is the RP for component A in both geometries. Its trend reveals both atomic and metallic contributions [indicated as "a" and "m" in Fig. 8(a)] to the wave function of the intermediate states involved in the de-excitation process: it keeps a constant value at lower photon energies, it suddenly decreases while approaching the Co 3p edge (the minimum is around 62 eV), and then it increases

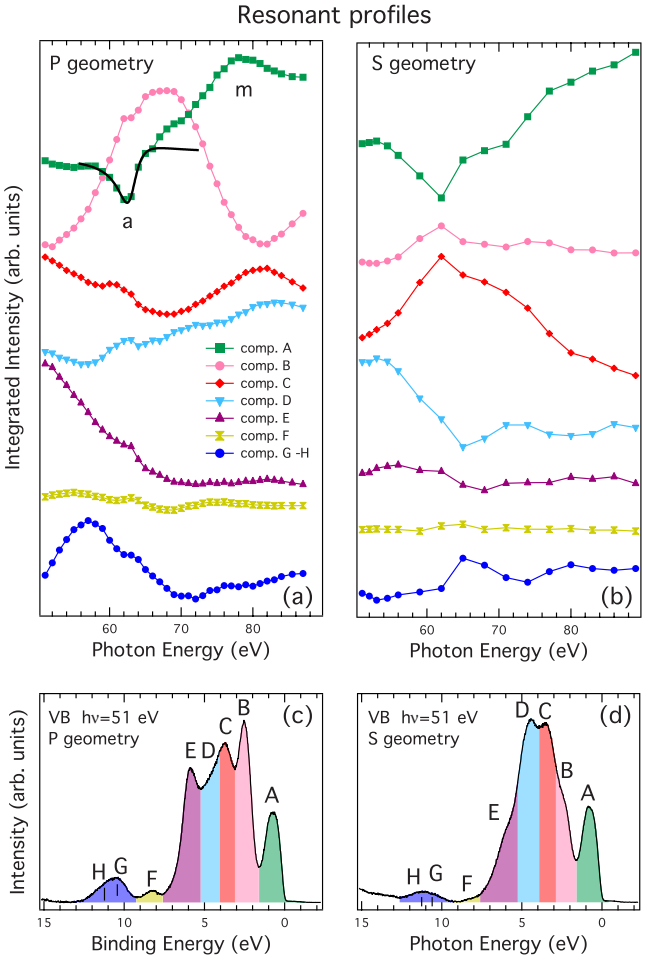

FIG. 8. (Color online) Resonant profiles for VB spectra acquired in (a) the P and S geometries. The resonant profiles have been calculated by integrating the VB spectra in different BE regions and normalizing to the overall VB intensity. The solid black line in (a) represents the Fano profile associated to the atomic part of the resonant profile. Panels (c) and (d) show the BE regions for the $h\nu$ =51 eV VB in P and S geometries, respectively (component A: 1.62 to −0.2 eV; component B: 3.1–1.62 eV; component C: 4.1–3.1 eV; component D: 5.25–4.1 eV; component E: 7.6–5.25 eV; component F: 9.25–7.6 eV ; and component G-H: 13–9.25 eV). The RP features are less smooth in the S geometry because fewer spectra were taken in this configuration.

moving to higher photon energies. The atomic part (from 58 to 66 eV) can be fitted with a Fano profile[39] (superimposed in the graph for the P geometry): a minimum close to the excitation threshold (~60 eV) and the following (relative) maximum, as a result of the interference between the wave functions of the electrons photoemitted directly from the VB or as a consequence of the autoionization. In the minimum, i.e., for destructive interference, the wave functions are out of phase. When approaching the maximum, the wave functions shift to the same phase, enhancing the total yield. The mathematical expression for the Fano profile is $I=(q+\epsilon)^2/(\epsilon^2+1)$, where q is the Fano asymmetry parameter and $\epsilon=(E-E_{th})/\Gamma$ (E_{th} is the resonance threshold energy and Γ is the lifetime width of the core level, Co 3p in this case). The fit gives $E_{th}=63$ eV, $\Gamma=1.5$ eV, and $q=0.36$. As q^2 is proportional to the ratio between the transition probabilities of indirect and direct PE processes, we can argue that emission A is dominated by the direct PE from the VB.

Together with this similarity with the atomic Fano resonance, two other characteristics can also be noticed corresponding to the resonant behavior of more delocalized states: first of all, the onset of the resonance maximum of this peak is delayed to ~78 eV, far above the 3p threshold; second, the resonance occurs over a broad energy range of more than 10 eV (as for components B and C in P and S geometries, respectively). Both the delay and the width of the resonance process are due to the metallic nature of unoccupied electron states above the Fermi level, which allow shake-up transitions from the VB to the empty states across several tens of eV, simultaneously with the excitation of a 3p core electron. Such a behavior is similar to that reported in literature for metallic Co.[40] The shoulder representing the atomic effects is absent in the RP of components B and C in P and S geometries, respectively. We ascribe this behavior to the more delocalized Co 3d wave functions in this energy region due to the hybridization with O 2p states.

While the RP for component F remains constant in the entire energy range for both geometries, the RPs for emissions D, E, and G-H have different trends in the P or S geometry. For D and E this could be due to the fact that these emissions are not clearly distinct in the VB. More interesting is the resonant behavior of the correlation satellite G, calculated by integrating the spectral intensity from 9.25 to 13 eV (we assume that Bi 6s intensity H is not affected by Co resonance). Its resonance maximum occurs at ~57 eV in the P geometry, slightly below the Co 3p core level maximum, and at ~65 eV in the S geometry, above the 3p absorption edge.

E. Photon energy dependence of the valence band

Figure 9(a) shows the modulation in intensity of the VB states as the photon energy is varied from 122 to 187 eV in the P geometry. The spectra were normalized with respect to the background at 50 eV BE. By taking advantage of the different dependences of the cross section on the photon energy between the Co 3d and the O 2p states, in particular below 200 eV [see Fig. 9(b)], we can discriminate the character of VB states by monitoring their relative intensity emissions versus the energy of the photon. We have limited the analysis to photon energies in the range of 100–200 eV, avoiding photon energies below 90 eV since the Co 3d cross section could be still affected by Co 3p-3d resonance interference effects.

A qualitative comparison of these four spectra reveals that component A varies slightly in intensity, whereas emissions B and C show a dramatic photon energy dependence. This suggests that B and C have an O 2p character, as in this photon energy range the O 2p cross section decays faster than that of the Co 3d. As was pointed out by the ResPES data at the Co M_{32} edges (Fig. 7), this is the energy region in which Co 3d states are also found. As emissions B and C are those that resonate at the Co M_{32} threshold in the P and S geometries, respectively, this finding can be regarded as an experimental evidence of the strong overlap between the

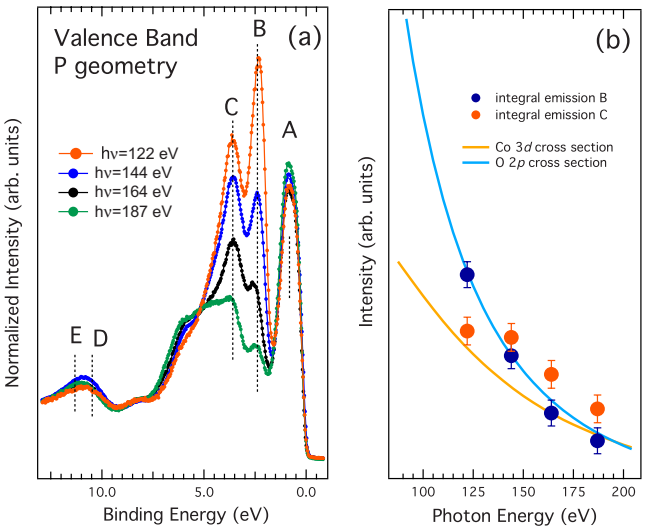

FIG. 9. (Color online) (a) VB PE spectra acquired at different photon energies in horizontal polarization. The overall resolution is 0.1 eV. The spectra have been aligned with respect to the Bi $5d_{5/2}$ core level and normalized at 50 eV BE. (b) The O $2p$ and Co $3d$ PE cross sections plotted as a function of the photon energy (taken from Ref. 41), normalized at 200 eV, together with the integrated intensity of emissions B and C.

O $2p$ and Co $3d$ orbitals. Moreover, emission C decays more slowly than B as the photon energy increases. In Fig. 9(b) the integral of components B and C superimposed on the Co $3d$ and O $2p$ cross sections[41] was reported. The integral of emission B follows quite well the decay of the O $2p$ cross section, while the integral of emission C does not. This behavior is consistent with the idea that emission B has more O $2p$ character than emission C. This is also consistent with the larger resonant increase in emission C at the Co M_{32} edges with respect to emission B [see Fig. 7(c)].

V. RAMAN-AUGER TRANSITION AND ESTIMATION OF THE CHARGE TRANSFER TIME

A. Transitions at the Co L_3 edge

The existence of Co L_3VV Auger emissions, which grow from $h\nu \simeq 777$ eV at 3.8 eV BE [i.e., ~767.5 eV kinetic energy (KE)] and resonate according to the absorption intensity, in Co L_3 ResPES spectra [see Fig. 5(a) and 5(b)] is due to the core hole recombination dynamics. In fact, the pure resonant states resonate at constant binding energy if the excited electron remains localized on the ion and it participates in the core hole decay.[42] However, when the excited electron delocalizes "before" the core hole recombination process (for example, via hopping to the ligand orbitals or to the conduction band), it does not participate in the core hole decay, and the system decays via a normal Auger process. As a consequence, the emitted electron is detected at constant kinetic energy. The transition from constant BE (Raman) to constant kinetic energy (normal Auger) emission occurs when the lifetime of the core hole (referred to also as the charge transfer time) becomes shorter than the lifetime of the intermediate state. So ResPES can also probe the degree of localization of resonating states and indirectly the time scale of the charge transfer processes of matter in the low-femtosecond time regimes, with an intrinsic lifetime scale given by the lifetime of the intermediate (core hole) state.[42,43] Obviously, the above description and its consequences are valid in the limit of the PE sudden approximation, in which the relaxation of the on-site electronic cloud due to the Coulomb potential created by the deep core hole is omitted.

Figure 10 shows the kinetic energy position of the Co L_3VV Auger peak as a function of the incident photon energy for both P and S geometries. The KE has been extracted by fitting the centroid of the Co L_3VV Auger with a Gaussian line shape. The error bars have been estimated from the fitting procedure. The Co L_3 XAS acquired in the P geometry has been superimposed in the graph for comparison. Well below the Co L_3 edge, the KE position changes with the photon energy. This behavior is typical of the nonradiative Raman regime, where the excited core electron participates in the core hole recombination process. The KEs of the Auger peak are different for the P and S geometries. As the difference is within the error bar, we cannot discriminate if this different slope originates from a geometrical factor or is an artifact. Moreover, in the Raman regime we observe little differences in the line shape of these peaks in the two geometries, which could be, in principle, ascribed to the different intermediate states selected by the polarization selection rules. However, we cannot unambiguously interpret these features because the Co L_3VV Auger overlap with the one-electron removal VB emission.

We have fitted this "pre-edge" region with a linear function ($y=a+bx$) giving $b=1.13\pm0.03$ for the P geometry and $b=1.010\pm0.015$ for the S geometry, consistent with that expected for Raman behavior. For $h\nu>778.5$ eV, the slope decreases and the KE reaches a maximum value of ~770.2 eV at $h\nu\sim779.3$ eV. This value corresponds to the BE of the Co $2p_{3/2}$ core level (E_B), which is about 0.6 eV higher than the KE value characteristic of the off-resonance Auger (769.615 ± 0.030 eV). At higher photon energies the position of the peak gradually moves toward lower KE values and reaches at ~780.2 eV (in correspondence of the maximum of the absorption edge, E_X) the kinetic energy of the off-resonant Auger spectra. The deviation from the Raman-like behavior takes place at the intersection between the pre-edge region and the above resonance regime at $h\nu$ ~778.5 eV, corresponding to Co $3d$ a_{1g} states of the absorption edge. This behavior is interpreted as a sudden delocalization of the excited electrons as soon as they have enough energy to reach Co $3d$ a_{1g} empty states.

The presence of an intermediate region between E_B and E_X, where the slope of the curve deviates from one, suggests an overlap between Raman and normal Auger processes, which could be the result of the persistence of reduced $3d$ electron localization as $h\nu$ is increased above the E_B value. When $h\nu$ reaches E_X, the system is free to de-excite through a pure normal Auger process. A similar behavior has been observed before for the Mn L_3VV Auger in Mn/Si(111) thin films.[44]

B. Transitions at the O K edge

Figures 11(a) and 11(b) show a selection of ResPES spectra obtained by tuning the photon energy across the O K edge

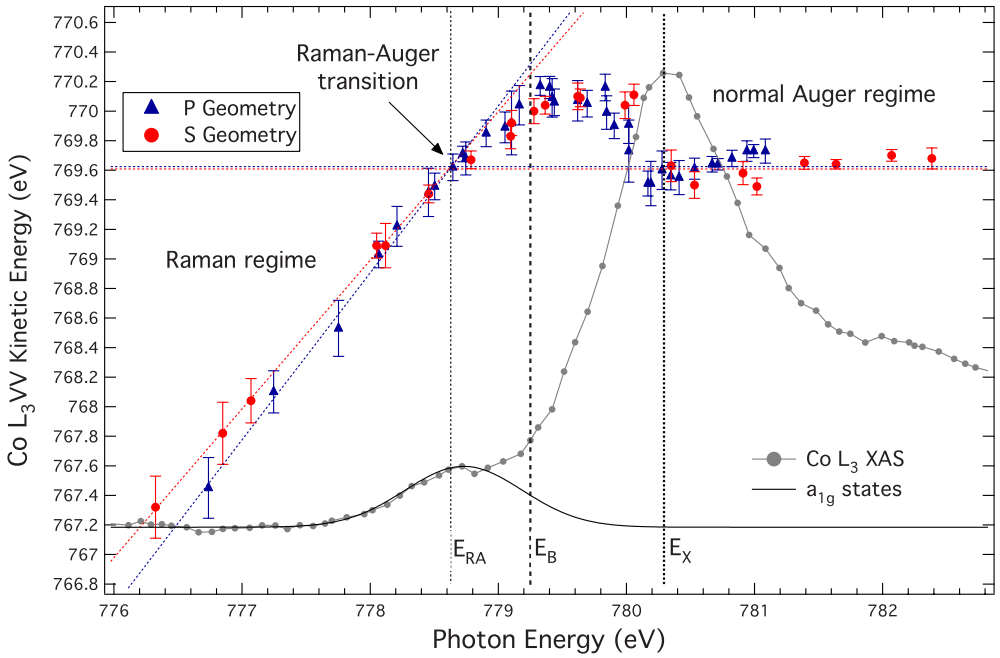

FIG. 10. (Color online) Kinetic energy position of the Co L_3VV Auger peak plotted as a function of the incident photon energy for both P (blue) and S (red) geometries. Co L_3 XAS acquired in the P geometry has been superimposed in the graph for comparison, together with a Gaussian representing Co a_{1g} states. The crossover is the energy of the intersection point of the two straight lines fitting the Raman and normal regimes (dashed lines). E_{RA}, E_B, and E_X are indicated by vertical dashed lines and their meanings are explained in the text.

from 523.5 to 535.25 eV in both geometries. The spectra have been normalized to the incident flux and plotted as a function of the kinetic energy for a better representation. The photon energies are marked as circles on the corresponding XAS spectra in (b) and (d). The VB and outer core levels (Bi 6*s*, O 2*s*, Ca 3*p*, Bi 5*d*, and Ca 3*s*) are visible together with four resonant Auger peaks (labeled as A–D, going from higher to lower kinetic energies). It is worth noting that emission A, originating from the O 1*s*2*p*2*p* Auger process, is derived from transitions that interfere with direct PE from the VB. Peaks B and C correspond to O 1*s*2*s*2*p* Auger transitions, while peak D corresponds to the O 1*s*2*s*2*s* Auger peak.[45] The intensity of these four Auger emissions changes while the photon energy is tuned across the absorption threshold according to the absorption intensity.

It is worth noting that no pure resonance in the VB appears while the photon energy is tuned across the absorption edge. There is an increase in spectral weight in the deeper part of the VB (from 2 to 7 eV BE) due to the low-BE tail of the O 1*s*2*p*2*p* Auger peak. This occurs because of the delocalized nature of the O 2*p* orbitals, causing the excited intermediate states to have a lifetime smaller than the lifetime of the O 1*s* core hole, so that all the electrons delocalize faster than the recombination process and no constructive interference can occur. This does not occur at the Co L_3 edges due to the more localized nature of some of the Co 3*d* intermediate states.

In the following we focus only on the O 1*s*2*p*2*p* Auger line, as B–D have lower intensities and other core levels are located in the same energy region. Tracking the KE position of the O 1*s*2*p*2*p* Auger peak is complicated as the Auger line shape is constituted by at least four components. Therefore, we have limited our analysis to photon energies at the beginning of the absorption edge, where the Raman-Auger transition takes place. In this energy region the Auger peak can be interpreted as a single component emission. Figure 12 shows a magnification of the O 1*s*2*p*2*p* Auger peak, while the photon energy is tuned across the O *K* edge in the energy range of 523.5–528.75 eV, in the S geometry. The Auger KE position is indicated by vertical dashes. Emission A undergoes a transition from a Raman regime to a normal-Auger regime, which takes place in correspondence to the thick green spectrum, acquired at $h\nu \sim 528.1$ eV (E_{RA}), in correspondence to the O 2*p* states hybridized with the Co a_{1g} state of the XAS spectrum, similarly to the Co L_3 edge. This photon energy is located 2 eV below the absorption edge maximum and 1 eV below the O 1*s* core level BE (529 eV). The transition takes place at $h\nu \sim 528$ eV in the P geometry (not shown here). As the monochromator resolution was set to 0.2 eV, the difference between these two values is within the experimental resolution, and no further details can be gained by the present data. We observe differences in the line shape of this peak in the two geometries, which are visible because the peaks do not overlap with valence-band states. The analysis of the O *K*VV Auger line shape as a function of the incident photon energy and polarization across the absorption threshold requires an extensive and detailed work that is out of the scope of this paper.

The charge transfer dynamics reported for O and Co Augers suggests a model for the electron transport based on Co a_{1g}–Co a_{1g} indirect hopping: an electron in a Co a_{1g} orbital can hop only onto the nearest Co atoms (into another a_{1g} orbital) through an intermediate O 2*p* orbital of suitable symmetry. In this sense the oxygen ligands are the mediators of the indirect exchange interaction between Co atoms. This mechanism thus realizes the macroscopic electron motion

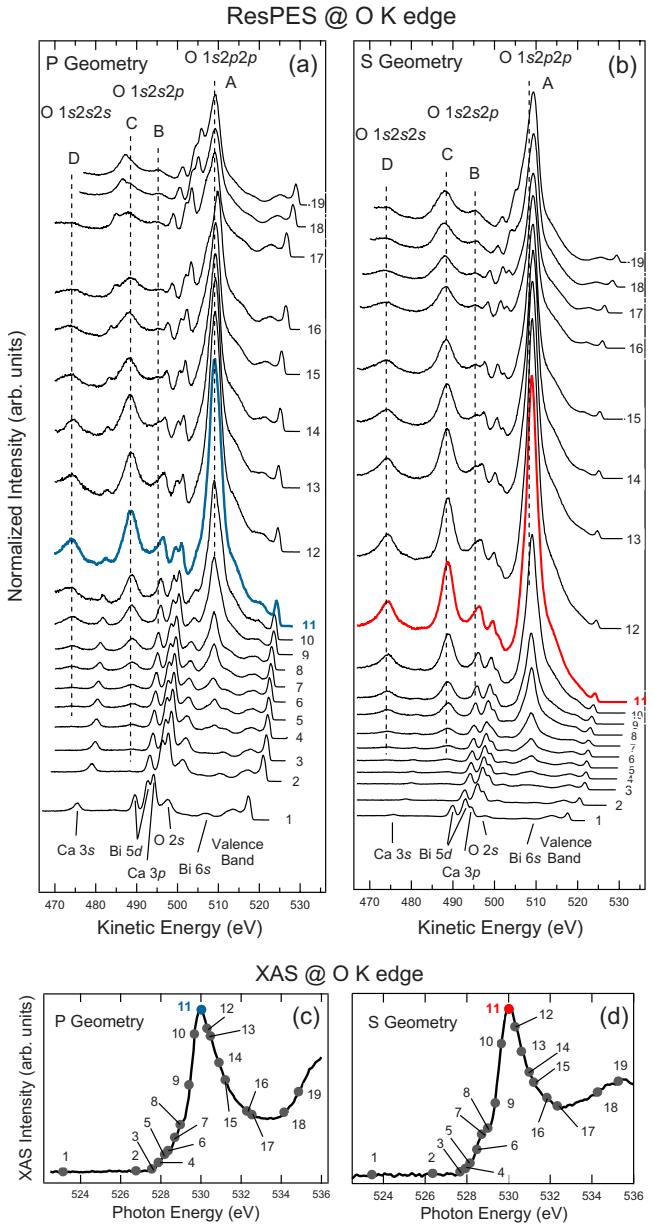

FIG. 11. (Color online) Selection of ResPES spectra at the O *K* edge acquired on BiCaCoO in the (a) P and (b) S geometries. The spectra corresponding to the resonance maximum are shown in thick line (blue and red, respectively). The spectra have been normalized to the incident flux. The incident photon energies are marked as full circles on the corresponding XAS spectra in (c) and (d), respectively. The blue and red circles indicate the photon energies at which the PE spectra were collected in the corresponding geometry. Peaks A–D that are marked by dashed lines correspond to oxygen Auger peaks as labeled in the graphs.

along the *ab* plane. Our results support the picture that the indirect overlap between Co 3*d* wave functions is predominant in the charge transport mechanism even if a direct Co-Co hopping cannot be excluded. This is supported by theoretical work[19,46] claiming that, even if the direct hopping between *d* electrons might be important for a realistic description of the band structure, its value is at least half that of the indirect hopping.

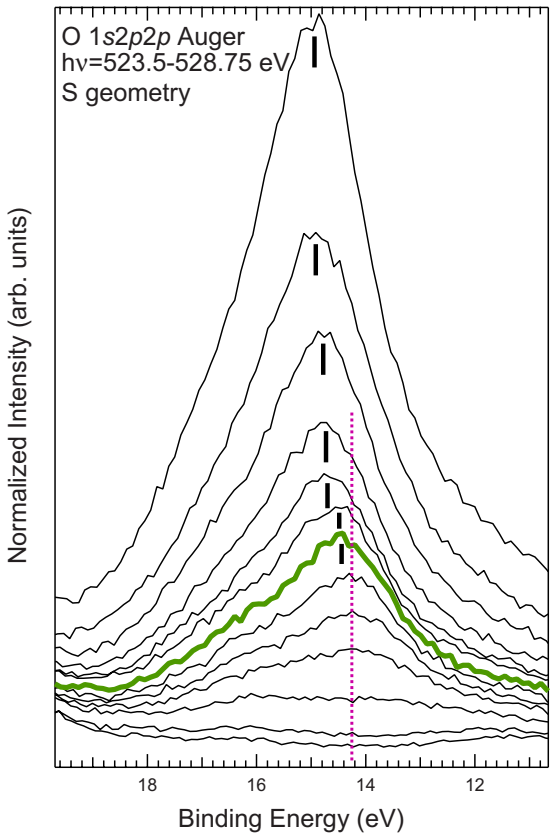

FIG. 12. (Color online) O 1*s*2*p*2*p* Auger peak acquired for $h\nu$ in an energy range from 523.5 to 528.75 eV in the S geometry. The spectra are plotted as a function of the BE. The thick green spectrum corresponds to the Raman-Auger transition ($h\nu$=528 eV). The purple line indicates the KE position in the Raman regime.

C. Charge transfer time

The transition from the Raman to the normal Auger regime is governed by the competition between the time scales corresponding to the core-hole decay (τ_{ch}) and the charge transfer (τ_{ct}) or, in more general terms, the delocalization of the excited core electron in the intermediate state. If $\tau_{ct} < \tau_{ch}$ the electron will hop on the ligand and the system will de-excite via normal Auger behavior. These rates are not simply constants, but they change throughout the absorption threshold. As was suggested by earlier measurements (see, for example, Ref. 47), the charge transfer time may possibly depend on the intermediate state. This is due to the excitations into orbitals hybridized with the neighboring atoms, which have higher probability of delocalization in a given time. On the other hand, close to the threshold, the core-hole decay time has to be replaced by an "effective scattering time," which depends on the photon energy relative to the absorption edge[43,48] according to

$$\tau_{ct} = \frac{1}{\sqrt{\Gamma^2 + \Omega^2}}, \tag{4}$$

where Ω is the detuning energy (the difference between the absorption edge maximum and the energy at which the Raman-Auger takes place) and Γ is the lifetime of the core

hole. The lifetime of the core hole could be, in principle, derived from a fit of the O 1*s* core level PE spectrum with a Voigt function fixing the Gaussian width equal to the overall experimental resolution. Unfortunately, we cannot fit the experimental spectra because of the complexity of the bonds between the oxygen and the metal ions. To give an estimation of the charge transfer time, we take the O 1*s* core hole lifetime from gas phase PE experiments. Prince *et al.*[49] showed that the O 1*s* core hole lifetime in different gases is similar and it corresponds to a bandwidth of ~0.15 meV. Assuming also for the present system a O 1*s* core hole lifetime of $\Gamma=0.15$ eV, with a detuning Ω of ~2 eV, from Eq. (4) we obtain $\tau_{ct}\sim 3.3$ fs for electron transfer from O 2*p* to Co 3*d* empty states, while $\tau_{ct}\sim 3$ fs for electron transfer from Co 3*d* to O 2*p* empty states. We do not think such a hopping could break the spin degeneracy (responsible for the large spin entropy and consequently for the high thermopower of this system)[4] because both spin channels are coupled through it in the same way.

The effect of the electron correlation on the interpretation of experimental photoemission data has been measured by Valla *et al.*[50] in the case of ARPES measurements for two parent compounds, namely, $NaCo_2O_4$ and Pb-doped Bi-Ba misfit cobaltates. The authors have pointed out how the merge of the quasiparticle peak near E_F while the temperature is decreased is a fingerprint of strong electronic correlations. However, this is not the case for the system under investigation here as ARPES measurements report the lack of the quasiparticle peak in BiCaCoO.[8]

VI. CONCLUSIONS

In conclusion, we have performed polarization-dependent PE, ResPES, and XAS on the Bi misfit cobaltate BiCaCoO. The present study unambiguously identifies the character of the VB states in the one-electron removal PE spectra. The occupied and empty states near E_F exhibit Co 3*d* (a_{1g}) character, while the emissions from the Co 3*d* states spans from E_F to ~4.5 eV below E_F, having a strong overlap with the O 2*p* states in the ~1.8–~4.5 eV BE energy region.

Concerning the de-excitation emissions, the Co $2p_{3/2}3d3d$ and O 1*s*2*p*2*p* Auger peaks undergo a transition from a Raman to a normal Auger regime by tuning the incident photon energy across the Co $2p_{3/2}\rightarrow$Co 3*d* (a_{1g}) threshold and the O 1*s*→O 2*p*–Co 3*d* (a_{1g}) hybridized threshold, respectively. In the limit of the sudden approximation, this result suggests a picture in which the electron hopping process between neighboring Co a_{1g} states across E_F is mediated by O 2*p* states with suitable symmetry.

The charge transfer times, estimated from the value of the detuning energy and the core hole lifetime [Eq. (4)], are ~3 fs for electrons from Co 3*d* to O 2*p* states and ~3.3 fs for electron transfer from O 2*p* to Co 3*d* states.

ACKNOWLEDGMENTS

The authors would like to thank Marco Zangrando for technical support during the experiments, Federica Bondino and Elena Magnano for determining the analyzer work function, and Bryan Doyle for helpful discussion.

*Present address: Department of Physics, University of Johannesburg, PO Box 524, Auckland Park 2006, South Africa.
†fulvio.parmigiani@elettra.trieste.it

[1] I. Terasaki, Y. Sasago, and K. Uchinokura, Phys. Rev. B **56**, R12685 (1997).
[2] A. C. Masset, C. Michel, A. Maignan, M. Hervieu, O. Toulemonde, F. Studer, B. Raveau, and J. Hejtmanek, Phys. Rev. B **62**, 166 (2000).
[3] M. Hervieu, A. Maignan, C. Michel, V. Hardy, N. Créon, and B. Raveau, Phys. Rev. B **67**, 045112 (2003).
[4] A. Maignan, S. Hébert, M. Hervieu, C. Michel, D. Pelloquin, and D. Khomskii, J. Phys.: Condens. Matter **15**, 2711 (2003).
[5] M. Lee, L. Viciu, L. Li, Y. Wang, M. L. Foo, S. Watauchi, R. A. Pascal, Jr., R. J. Cava, and N. P. Ong, Nature Mater. **5**, 537 (2006).
[6] Y. F. Hu, W. D. Si, E. Sutter, and Q. Li, Appl. Phys. Lett. **86**, 082103 (2005).
[7] G. J. Snyder and E. S. Toberer, Nature Mater. **7**, 105 (2008).
[8] V. Brouet, A. Nicolaou, M. Zacchigna, A. Tejeda, L. Patthey, S. Hébert, W. Kobayashi, H. Muguerra, and D. Grebille, Phys. Rev. B **76**, 100403(R) (2007).
[9] G. Xu, R. Funahashi, M. Shikano, M. Matsubara, and Y. Zhou, J. Appl. Phys. **91**, 4344 (2002).
[10] W. Kobayashi, H. Muguerra, S. Hébert, D. Grebille, and A. Maignan, 26th International Conference on Thermoelectrics, ICT 2007.
[11] J. Bobroff, S. Hébert, G. Lang, P. Mendels, D. Pelloquin, and A. Maignan, Phys. Rev. B **76**, 100407(R) (2007).
[12] P. Limelette, S. Hébert, H. Muguerra, R. Frésard, and C. Simon, Phys. Rev. B **77**, 235118 (2008).
[13] Y. Tanaka, T. Fujiia, M. Nakanishia, Y. Kusanob, H. Hashimotoa, Y. Ikedac, and J. Takadaa, Solid State Commun. **141**, 122 (2007).
[14] X. Luo, Y. Jing, H. Chen, and X. Chen, J. Cryst. Growth **308**, 309 (2007).
[15] D. Grebille, H. Muguerra, O. Pérez, E. Guilmeau, H. Rousselière, and R. Funahashi, Acta Crystallogr., Sect. B: Struct. Sci. **63**, 373 (2007).
[16] S. Landron and M.-B. Lepetit, Phys. Rev. B **74**, 184507 (2006).
[17] I. Tsukada, T. Yamamoto, M. Takagi, T. Tsubone, S. Konno, and K. Uchinokura, J. Phys. Soc. Jpn. **70**, 834 (2001).
[18] T. Yamamoto, K. Uchinokura, and I. Tsukada, Phys. Rev. B **65**, 184434 (2002).
[19] W. Koshibae and S. Maekawa, Phys. Rev. Lett. **91**, 257003 (2003).
[20] D. J. Singh, Phys. Rev. B **61**, 13397 (2000).
[21] T. Mizokawa, L. H. Tjeng, P. G. Steeneken, N. B. Brookes, I. Tsukada, T. Yamamoto, and K. Uchinokura, Phys. Rev. B **64**, 115104 (2001).
[22] M. Kubota *et al.*, Phys. Rev. B **70**, 012508 (2004).
[23] J.-S. Kang, S. W. Han, T. Fujii, I. Terasaki, S. S. Lee, G. Kim, C. G. Olson, H. G. Lee, J.-Y. Kim, and B. I. Min, Phys. Rev. B **74**,

205116 (2006).
[24] M. Z. Hasan *et al.*, Phys. Rev. Lett. **92**, 246402 (2004).
[25] H.-B. Yang *et al.*, Phys. Rev. Lett. **95**, 146401 (2005).
[26] D. Qian, L. Wray, D. Hsieh, L. Viciu, R. J. Cava, J. L. Luo, D. Wu, N. L. Wang, and M. Z. Hasan, Phys. Rev. Lett. **97**, 186405 (2006).
[27] D. Qian *et al.*, Phys. Rev. Lett. **96**, 046407 (2006).
[28] Z. Yusof, B. O. Wells, T. Valla, P. D. Johnson, A. V. Fedorov, Q. Li, S. M. Loureiro, and R. J. Cava, Phys. Rev. B **76**, 165115 (2007).
[29] S. Landron and M.-B. Lepetit, Phys. Rev. B **77**, 125106 (2008).
[30] H. Leligny, D. Grebille, O. Pérez, A. Masset, M. Hervieu, and B. Raveau, Acta Crystallogr., Sect. B: Struct. Sci. **56**, 173 (2000).
[31] M. Zangrando, M. Finazzi, G. Paolucci, G. Comelli, B. Diviacco, R. P. Walker, D. Cocco, and F. Parmigiani, Rev. Sci. Instrum. **72**, 1313 (2001).
[32] M. Zangrando, M. Zacchigna, M. Finazzi, D. Cocco, R. Rochow, and F. Parmigiani, Rev. Sci. Instrum. **75**, 31 (2004).
[33] W. B. Wu, D. J. Huang, J. Okamoto, A. Tanaka, H.-J. Lin, F. C. Chou, A. Fujimori, and C. T. Chen, Phys. Rev. Lett. **94**, 146402 (2005).
[34] T. Kroll, M. Knupfer, J. Geck, C. Hess, T. Schwieger, G. Krabbes, C. Sekar, D. R. Batchelor, H. Berger, and B. Buchner, Phys. Rev. B **74**, 115123 (2006).
[35] M. Malvestuto (unpublished).
[36] T. Mizokawa, New J. Phys. **6**, 169 (2004).
[37] T. Takeuchi *et al.*, Phys. Rev. B **69**, 125410 (2004).
[38] D. A. Shirley, Phys. Rev. B **5**, 4709 (1972).
[39] U. Fano, Phys. Rev. **124**, 1866 (1961).
[40] T. Kaurila, J. Väyrynen, and M. Isokallio, J. Phys.: Condens. Matter. **9**, 6533 (1997).
[41] J.-J. Yeh, *Atomic Calculation of Photoionization Cross-Sections and Asymmetry Parameters* (Gordon and Breach, Langhorne, PA, 1993).
[42] P. A. Brühwiler, O. Karis, and N. Mårtensson, Rev. Mod. Phys. **74**, 703 (2002).
[43] H. Agren and F. Gel'mukhanov, J. Electron Spectrosc. Relat. Phenom. **110-111**, 153 (2000).
[44] M. Zangrando, E. Magnano, A. Nicolaou, E. Carleschi, and F. Parmigiani, Phys. Rev. B **75**, 233402 (2007).
[45] M. Finazzi and N. B. Brookes, Phys. Rev. B **60**, 5354 (1999).
[46] A. Bourgeois, A. A. Aligia, T. Kroll, and M. D. N. nez Regueiro, Phys. Rev. B **75**, 174518 (2007).
[47] O. Karis, A. Nilsson, M. Weinelt, T. Wiell, C. Puglia, N. Wassdahl, N. Mårtensson, M. Samant, and J. Stöhr, Phys. Rev. Lett. **76**, 1380 (1996).
[48] F. Gel'mukhanov and H. Agren, Phys. Rep. **312**, 87 (1999).
[49] K. Prince, M. Vondrácek, J. Karvonen, M. Coreno, R. Camilloni, L. Avaldi, and M. de Simone, J. Electron Spectrosc. Relat. Phenom. **101-103**, 141 (1999).
[50] T. Valla *et al.*, Nature (London) **417**, 627 (2002).